10

Enhanced Electro-Optical Properties of Liquid Crystals Devices by Doping with Ferroelectric Nanoparticles

Hao-Hsun Liang and Jiunn-Yih Lee
Department of Materials Science and Engineering, National Taiwan University of Science and Technology
The Republic of China at Taiwan

1. Introduction

Over the past few decades, liquid crystal (LC) displays (LCDs) have been at the leading edge of their field. Many scientists and manufacturers have devoted studies to improve the performance of LCD characteristics such as a fast response, high contrast ratio, and wide viewing angle. Therefore the in-plane switching (IPS) mode (Oh-e et al., 1995) was developed for wide viewing angle; vertical alignment (VA) mode for a higher contrast ratio; and ferroelectric (Clark et al., 1980; Meyer et al., 1975) and antiferroelectric LC (Chandani et al., 1988, 1989) for faster responses, instead of the common nematic LC and twist nematic (TN) modes. Recent studies of liquid crystals doped with nanoparticles have given rise to a number of novel practical applications and pointed the way toward innovative improvement of the physical and electro-optical properties of liquid crystal by means of chemical synthesis (Kobayashi & Toshima, 2007).

Enhancement of the electro-optical properties of liquid crystal is dependent on the size, type, concentration, and intrinsic characteristics of the nanoparticles used for doping. The nanoparticles should share similar attributes to the liquid crystal molecules and be of a size that would not significantly disrupt the order of the liquid crystal. Low doping concentrations (<3% by weight) are usually chosen to yield a more stable and even distribution in the liquid crystal, which lowers the interaction forces between particles.

Commonly used doping nanoparticles include ferromagnetic nanoparticles, metallic nanoparticles, inorganic nanoparticles, and ferroelectric nanoparticles. In the case of ferromagnetic nanoparticles, the large permanent magnetic moments couple with the LC direction, leading to improvements in their magnetic properties. This is known as ferronematics (Brochard & Gennes, 1970). In the case of metallic nanoparticles, due to the surface plasmon resonance and depolarization of the electric field, the metallic nanoparticles can enhance the memory effect of the ferroelectric liquid crystal (FLC) (Kaur et al., 2007) and dielectric properties of nematic liquid crystal (NLC) (Miyama et al., 2004; Shiraki et al.,2004). In the case of inorganic nanoparticles, their intrinsic structures can affect the vertical alignment without the need for an alignment layer (Jeng et al., 2007). Due to the large permanent dipole moments, ferroelectric nanoparticles induce realignment of neighboring liquid crystal molecules, thereby increasing the order parameter and lowering the threshold voltage (Reznikov et al., 2003).

Schurian and Bärner discovered that doping ultra-fine (less than 1 μm) dielectric particles into an isotropic liquid enhances its sensitivity to electric field (Schurian & Bärner, 1996); this heralded studies into the doping of ferroelectric nanoparticles ($BaTiO_3$, $Sn_2P_2S_6$) into NLC (Cheon et al., 2005; Kaczmarek et al., 2008; Li et al., 2006, 2006). Doping of nanoparticles was initially restricted to NLCs due to their widespread applications, technological maturity, and relatively simple liquid crystal structure (which allows the doping of nanoparticles to be less likely to destroy the alignment of the liquid crystal molecules). After the successful enhancement of the electro-optical properties of NLC, attention has turned to other candidates, such as cholesteric liquid crystal and smectic liquid crystal. In the case of cholesteric liquid crystals, there were significant improvements in the contrast of reflectance of planar-focal conic state, and driving voltage of the cholesteric liquid crystal after doping with ferroelectric nanoparticles. In the case of SmA liquid crystals, there were also significant improvements in the driving voltage (Glushchenko et al., 2006).

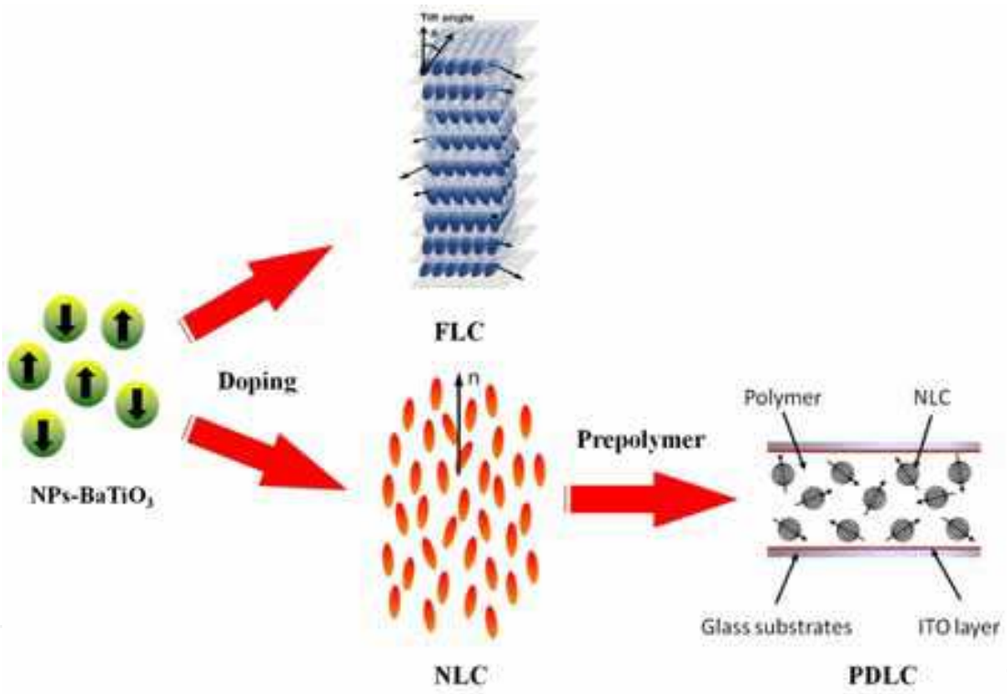

Fig. 1. Schematic representation of the proposed LC devices doped with ferroelectric $BaTiO_3$ nanoparticles.

Among all LC devices, the surface stabilised ferroelectric liquid crystal (SSFLC) mode, prepared using FLC, and the polymer dispersed liquid crystals (PDLC) mode, prepared using NLC, have received the most attention. By using an alignment layer and sufficiently thin cell gap (d <P, the helix pitch) to inhibit the formation of helical structures, the SSFLC structured device has many advantages including an enhanced memory effect, microsecond response time, and wide viewing angle (Lagerwall, 1999). On the other hand, PDLC light shutters combine the superior characteristics of both LCs and polymers, which provide several advantages: they require no polarizer, have fast response times, and can easily be fabricated into a large, flexible display (Crawford & Žumer, 1996; Drzaic, 1998). These are currently the most commonly used in switchable windows in modern buildings. However,

these two modes of light shutters still possess minor issues. In the case of SSFLC mode, the spontaneous polarization (P_s) value is an important factor when considering the response time of the light shutter, and often improvement can only be made via chemical synthesis; the PDLC mode has shortcomings including a high driving voltage and off-axis haze.
The content of this chapter focuses on the improvement of the electro-optical performance of two types of LC materials (FLC, NLC) by doping with ferroelectric $BaTiO_3$ nanoparticles (NPs-$BaTiO_3$). As shown in figure 1, the ferroelectric nanoparticles were well dispersed in the FLC and NLC respectively via appropriate wet grindings. By filling into the homogeneous cells, the former became a SSFLC mode; the latter formed an electrically controlled birefringence (ECB) mode. Subsequently, the addition of UV-curable prepolymer to fill the untreated substrate surface of the cell meant that the PDLC mode consisted of NLC, NPs-$BaTiO_3$ and the polymer. We introduced NPs-$BaTiO_3$ with a large electric dipole moment into the LC in order to enhance the physical properties (liquid crystal phase performance, dielectric properties, spontaneous polarization) and the electro-optical performance (V-T characteristics, and response time). Moreover, in the case of the PDLC mode, part of the NPs-$BaTiO_3$, coated by the polymer, can modify the refractive index of the polymer during phase separation, in order to increase the viewing angles of the 'field-on state' and reduce the off-axis haze effect.

2. Experiments

The characterization of materials (NPs-$BaTiO_3$, FLC, NLC, and prepolymer), sample preperation of NPs-$BaTiO_3$/ LC/polymer composites, and the measurements of the physical and electro-optical properties are described in this section.

2.1 Materials characterization

We made use of commercially available $BaTiO_3$ nanoparticles with an average size of 30-50 nm, polyhedron particle shapes (99+%, from Aldrich), tetrahedral crystal structure, [001] polar axis and a spontaneous polarization of 26 μC/cm² at room temperature. The dielectric constant of the $BaTiO_3$ single crystal is 168 in the direction parallel to the polar axis and 2,920 in the direction perpendicular to the polar axis. In contrast to other studies, which used oleic acid as the surfactant and heptane as the solvent, we made use of a solution of polymeric dispersant as a surfactant, taking advantage of the steric effect where the polymer chains stick to the ferroelectric nanoparticles enhance the dispersion. For the solvent, we used tetrahydrofuran (THF). The phase transition temperatures of the FLC CS1024 (fromChisso) we used are as follows: Cr $\underset{}{\overset{-12^{\circ}C}{}}$ SmC* $\underset{}{\overset{62^{\circ}C}{}}$ SmA $\underset{}{\overset{83^{\circ}C}{}}$ N* $\underset{}{\overset{93^{\circ}C}{}}$ Iso. At 25 °C, the spontaneous polarization was -46.9nC/cm² while the tilt angle was 25 degrees. The NLC DN113245 (from Daily Polymer) with positive dielectric anisotropic of $\Delta\varepsilon$=13.03 and birefringence Δn=0.24 at 25 °C exhibits a thermotropic transition sequence of Cr $\underset{}{\overset{-32^{\circ}C}{}}$ N $\underset{}{\overset{83^{\circ}C}{}}$ Iso. The UV-curable prepolymer NOA65 (from Norland Optical Adhesive) with a refractive index of n_p=1.52 (the same as the NLC) was employed for polymerization induced phase separation.

2.2 Sample preparation

We used wet grinding dispersion equipment and yttria-stabilized zirconia (YSZ) as the grinding media. The commercially available ferroelectric $BaTiO_3$ nanoparticles, polymeric

surfactant and THF were evenly mixed according to the weight ratio of 1: 0.15: 11. YSZ beads of the appropriate size were then chosen for 2 hour wet grinding. After ultrasonic dispersion, the $BaTiO_3$ suspension was added into FLC and NLC, and a vacuum was employed to evaporate the THF. After ultrasonic dispersion for an hour, we successfully prepared samples with different doping concentrations: Pure FLC, FLC+0.1wt% $BaTiO_3$. FLC+1wt% $BaTiO_3$, pure NLC, NLC+0.1wt% $BaTiO_3$, and NLC+0.5wt% $BaTiO_3$. The homogenous cells consisted of two indium tin oxide (ITO) coated glass substrates with a polyimide (PI) layer rubbed in anti-parallel directions to obtain the homogeneous alignment. The 2 μm and 4 μm homogeneous cells, which were controlled by dispersion of cylindrical glass spacers, were filled with $BaTiO_3$ doped FLC and $BaTiO_3$ doped NLC at above both clearing temperatures $T=95^oC > Tc$, to produce the surface stabilized ferroelectric liquid crystal (SSFLC) and electrically controlled birefringence (ECB) modes. For fabrication of PDLC, the NOA65, equivalent to NLC, was added to the $BaTiO_3$ doped NLC. The NLC- $BaTiO_3$/prepolymer mixture was injected into an empty cell whose inner surfaces were coated with a thin indium-tin-oxide (ITO) electrode. The cell gap was measured to be d=16 μm. The filled cell was then exposed to 3 minutes of UV light (20 mW/cm^2) at room temperature for polymerization induced phase separation (PIPS) to obtain the PDLC devices.

2.3 Instruments

The dispersion was implemented by a wet grinding dispersion equipment (Just Nanotech, JBM-B035). Particle size analyzers (PSA, Brookhaven 90Plus/BI-MAS) and a transmission electron microscope (TEM, JEOL 2000FXII) were used for the measurement of the size distribution of the $BaTiO_3$ nanoparticles. Polarizing optical microscopy (POM, OLYMPUS Optical Co., Ltd., Models BHSP-2, BX-51) was used to observe the liquid crystal phases, differential scanning calorimeter (DSC, PerkinElmer PYRIS 1) for the identification of the liquid crystal phase transition temperatures, scanning electron microscopy (SEM, Leica LEO 420) for PDLC morphology analysis, and low frequency impendence analysis (LFIA, Hewlett Packard 4192A) for measuring the dielectric properties. A Fourier transform infrared (FTIR) spectrometer, mass spectrometer (Finnigan TSQ- 700), and an elemental analyzer (HERAEUS Vario EL-III) were used for qualitative. To determine the value of the spontaneous polarization, we used triangular wave measurements (Miyasato et al, 1983).

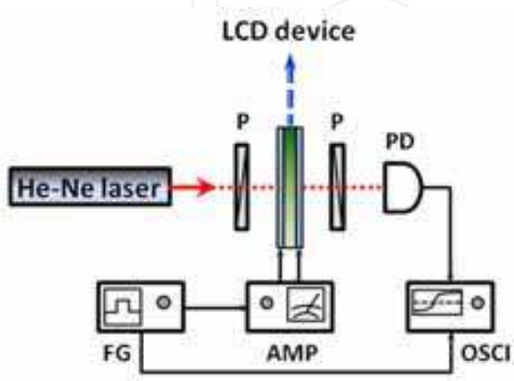

Fig. 2. Experimental setup for measuring the electro-optical properties of the LCD devices with an applied AC voltage. P, PD, FG, AMP, and OSCI represent polarizer, photodiode detector, function generator, high-voltage amplifier, and oscilloscope, respectively.

The electro-optical properties, shown in Figure 2, were obtained using a He-Ne laser (632.8nm, 10mW) as a light source, with orthogonal polarizers either side of the PDLC samples, and the light transmitted through the sample was collected by a photodiode (PD). The electrical signal from the PD was fed to an oscilloscope (OSCI). The AC electric field was supplied by a function generator (FG) in conjunction with a high-voltage amplifier (AMP).

3. Results and discussions

3.1 Identification of the host LC materials and NPs-$BaTiO_3$ after sample preparation

Vacuum treatment was used to remove the solvent (heptane), which could possibly result in the loss of lower molecular weight components in the nematic liquid crystal (Li et al, 2007). To ensure the experiment isolated the effects of the addition of nanoparticles, we performed qualitative and quantitative analysis to ascertain that the composition of the FLC and NLC mixture before and after vacuum treatment, and found that it did not change. The former involved the use of a FTIR spectrometer and mass spectrometer whereas the latter utilized elemental analyzer measurements. The qualitative and quantitative results confirmed that the composition of the FLC CS1024 and NLC DN113245 mixtures was unchanged after vacuum treatment. Combining both the qualitative and quantitative analyses, we can conclude that the changes in the electro-optical properties were entirely the result of the contribution from the $BaTiO_3$ suspension and not due to changes in the composition of the host LC materials during the preparation process.

Before doping, the PSA and TEM were used to determine the particle size distribution of the $BaTiO_3$ nanoparticles. After wet grinding to create the $BaTiO_3$ suspension, we added THF to yield a diluted 0.15 wt% $BaTiO_3$ suspension and performed particle size analysis using the dynamic light scattering technique. Figure 3 (a) shows the results of the PSA measurement, with 99% of the $BaTiO_3$ particles having a diameter of less than 100 nm. The mean diameter was 39.9 nm. Figures 3 (b) and (c) show the TEM measurements before and after grinding. In Figure 3 (b), the average $BaTiO_3$ particle size before grinding was about 90 nm; whereas in Figure 3 (c), the average $BaTiO_3$ particle size after grinding was about 31 nm. This indicates that the wet grinding and dispersion had successfully disrupted the aggregation of the nanoparticles, yielding a optimal nanoscale for ease of doping.

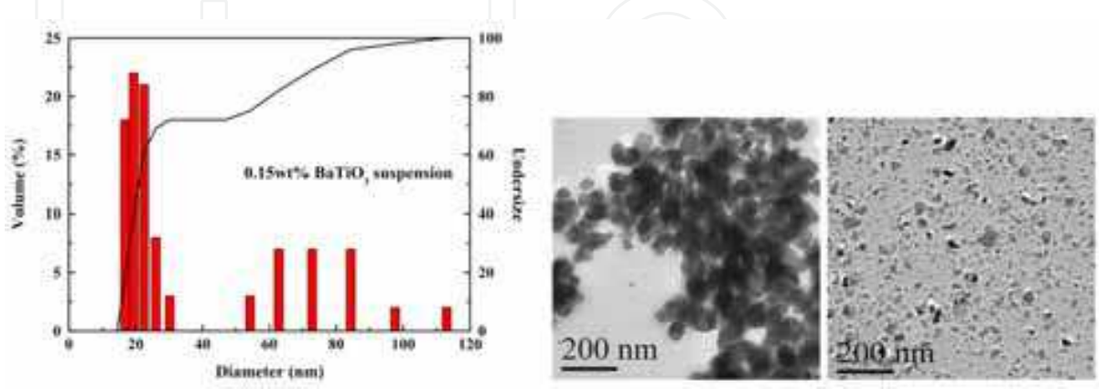

(a) (b) (c)

Fig. 3. (a) The results of the PSA measurement of 0.15wt% $BaTiO_3$ suspension. Transmission electron micrographs of $BaTiO_3$ nanoparticles (a) before and (b) after wet grinding.

3.2 Effect of doping NPs-$BaTiO_3$ on the physical and electro-optical properties of SSFLC mode

The range of liquid crystal phase transition temperatures after doping were measured by POM and DSC. Since the FLC material, CS1024, is a compound whose phase transition temperature is unlike a single component liquid crystal material, it is particularly hard to discern, especially for the SmA and SmC* phase transitions. Table 1 shows the phase transition temperatures of FLC with different doping concentrations. We can see that the pure FLC and FLC+0.1wt% $BaTiO_3$ had almost identical phase transition temperatures at $T_{N^*\text{-}I}$, $T_{N^*\text{-}SmA}$, $T_{SmA\text{-}SmC^*}$, whereas there were slight decreases in the various phase transition temperatures of the FLC+1.0 wt% $BaTiO_3$. In particular, there was a decrease of about 4 °C for the phase transition temperature of $T_{SmA\text{-}SmC^*}$. This result can alternatively be verified by measurements of the dielectric properties and spontaneous polarization.

Sample	Phase transition temperature
pure FLC	SmC* $\xleftrightarrow{61.15^oC}$ SmA $\xleftrightarrow{82.58^oC}$ N* $\xleftrightarrow{90.35^oC}$ Iso
FLC+0.1wt%$BaTiO_3$	SmC* $\xleftrightarrow{61.01^oC}$ SmA $\xleftrightarrow{82.35^oC}$ N* $\xleftrightarrow{90.12^oC}$ Iso
FLC+1.0wt%$BaTiO_3$	SmC* $\xleftrightarrow{56.78^oC}$ SmA $\xleftrightarrow{81.89^oC}$ N* $\xleftrightarrow{89.68^oC}$ Iso

Table 1. The phase transition temperature of FLC with different doping concentrations of $BaTiO_3$ suspensions.

After infusing the pure FLC and the FLC suspension into a 2 μm liquid crystal cell to create a SSFLC mode, one can observe the texture of the higher doping concentration FLC+1.0wt% $BaTiO_3$ under 200 times POM magnification (Figure 4). One can see clearly that there exists almost no characteristic texture of SmC*, indicating that we had successfully created a SSFLC mode. Other samples with different doping concentrations exhibited similar textures.

Fig. 4. The SSFLC texture of the FLC+1wt% $BaTiO_3$ at 30°C, under 200 times POM magnification. (The red arrow indicates the PI alignment rubbing direction)

To investigate the effect of doping concentration on the spontaneous polarization, we adopted a two-pronged approach: varying the applied voltage at a constant temperature and varying the temperature at the saturation voltage, using the triangular wave measurements for samples with different doping concentrations. Figure 5 shows the relationship between the temperature and spontaneous polarization for different doping concentrations of $BaTiO_3$ suspensions at f=10 Hz and V_{p-p}=20 V. The horizontal axis is the phase transition temperature from SmA to SmC*, for samples with different doping concentrations. We can see that the spontaneous polarization increased rapidly without reaching a maximum as the temperature was cooled to the SmC* phase. In order to understand the sensitivity of the applied voltage by the doping concentration, we attempted to fix the temperature at 35 °C in the SmC* liquid crystal phase, apply triangular waves with identical frequency (f=10 Hz) but different voltages and observe the relationship between the voltage and spontaneous polarization for different doping concentrations of $BaTiO_3$ suspensions (Figure 6). We can see a significant increase in the absolute values of the spontaneous polarization. The P_s of the FLC+0.1 wt% $BaTiO_3$ (slope=14.47099) and FLC +1.0wt% $BaTiO_3$ (slope=31.21684) also increased with the applied voltage. The slopes for the P_s values were also greater than those of pure FLC (slope=10.10697). This further proves that the doping had significantly improved the sensitivity of the FLC under an applied electric field. In particular, the FLC+0.1 wt% $BaTiO_3$ exhibited the largest spontaneous polarization, even reaching a value that is twice that of pure FLC (80 nC/cm²).

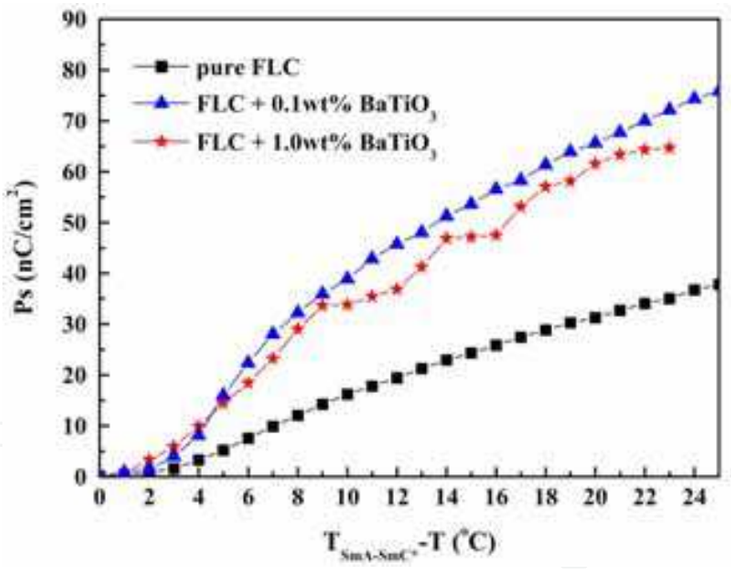

Fig. 5. The dependence of the spontaneous polarization for FLC with different doping concentrations of $BaTiO_3$ suspensions on the temperature at f=10Hz and V_{p-p}=20V.

Assuming that the P_s resulted from the contributions of the $BaTiO_3$ and FLC, we can apply the zeroth order approximation to estimate the P_s value after doping:

$$P_s^{susp.} = (1 - f_w) P_s^{LC} + f_w P_s^{particles} \tag{1}$$

where f_w is the weight ratio of the $BaTiO_3$ suspension. Using the above formula, one obtains a P_s value of about 68 nC/cm² for the lower doping concentration FLC+0.1 wt% $BaTiO_3$ and

about 300 nC/cm² for the higher doping concentration FLC+1.0wt% $BaTiO_3$ These calculated values are much higher than the experimental value of 65 nC/cm². One possible explanation for the discrepancy is that when the interactions between particles were ignored, the larger size of the nanoparticles than the liquid crystal molecules led to disruption of the FLC stacking, resulting in a smaller P_s value than expected.

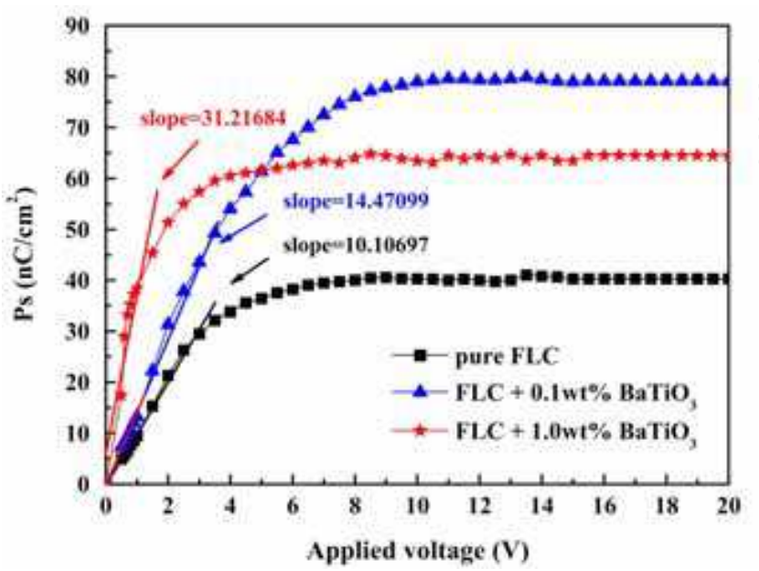

Fig. 6. The dependence of the spontaneous polarization for FLC with different doping concentrations of $BaTiO_3$ suspensions on the applied voltage at 35°C

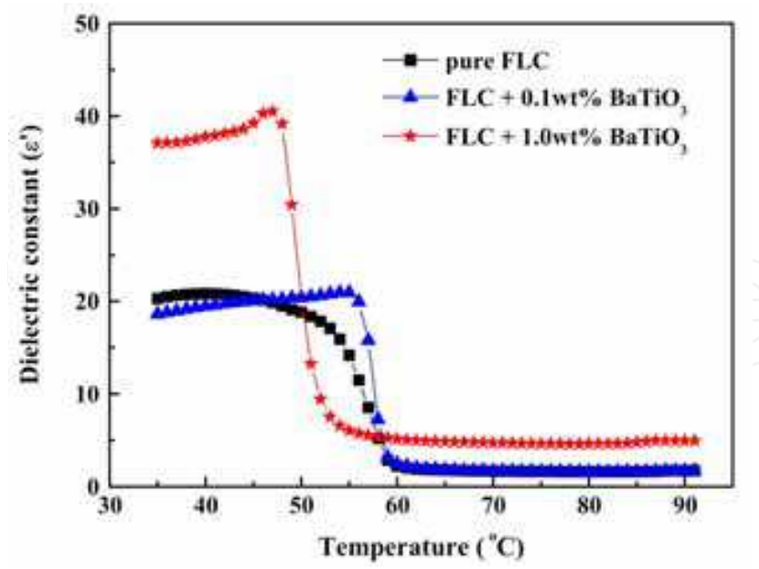

Fig. 7. The dependence of the dielectric constant (ε') for FLC with different doping concentrations of $BaTiO_3$ suspensions on the temperature at 1 kHz.

Figure 7 shows the relationship between the permittivity and the temperature of the pure FLC, FLC+0.1wt% $BaTiO_3$ and FLC+1.0wt% $BaTiO_3$ at a frequency of 1 kHz. The

permittivity increased drastically when cooling to 60 °C in the SmC* phase. We can see from Figure 7 that there was very little difference in the permittivity for the different liquid crystal phases of pure FLC and FLC+0.1 wt% $BaTiO_3$ whereas the permittivity of the various liquid crystal phases of FLC+1.0 wt% $BaTiO_3$ were twice those of the others. In particular, the maximum permittivity, 42.9, occurred at 49 °C while the average permittivity of its SmC* phase was approximately 1.5 times those of the pure FLC and FLC+0.1wt% $BaTiO_3$ Therefore, one can see that the doping of $BaTiO_3$ effectively enhanced the permittivity of the liquid crystal material with its large electric dipole moment. In addition, one can also observe the significant differences in the slopes of the permittivity curves when the pure FLC, FLC+0.1wt% $BaTiO_3$ and FLC+1.0wt% $BaTiO_3$ samples entered the SmC* phase. A comparison of the pure FLC and FLC+0.1wt% $BaTiO_3$ revealed that while there was little difference between the permittivity, there was a very significant increase in the slope of the permittivity curve. The effect was especially prominent in the FLC+1.0 wt% $BaTiO_3$, thereby further affirming the observations regarding spontaneous polarization. The doping of NPs-$BaTiO_3$ into the liquid crystal material had enhanced their sensitivity to applied electric fields, and the permittivity curve exhibited a rapid increase upon entering the SmC* phase, before rising to the maximum value.

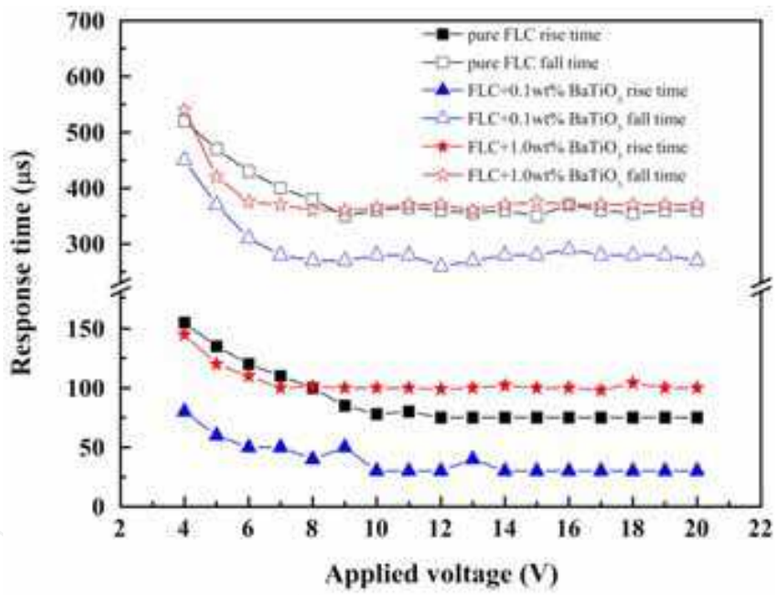

Fig. 8. The dependence of response time for FLC with different doping concentrations of $BaTiO_3$ suspensions on the applied electric field.

To investigate the response time of the SSFLC mode, V_{p-p} = 20 V, f =10 Hz was applied at a constant temperature of 35 °C. Figure 8 shows the relationship between the applied voltage and the response time. One can see that the response time for the pure FLC, FLC+0.1 wt% $BaTiO_3$ and FLC+1.0wt% $BaTiO_3$ decreased rapidly before saturating with increased applied voltage. This is evidence that the response time will saturate regardless of the applied voltage once the saturation voltage had been exceeded. The response times for all three are tabulated in Table 2. The FLC+1.0 wt% $BaTiO_3$ had the minimum rise and fall times. The rise and fall time values in descending order were found in FLC+1.0 wt% $BaTiO_3$, pure FLC and FLC+0.1 wt% $BaTiO_3$. The response time is the sum of the rise and fall times, and took

values of 435 μs, 310 μs and 470 μs, with increased doping concentrations. In addition, from Equation (Kimura et al, 1987):

$$\tau^{-1} = \frac{\tau P_s E}{1.76\gamma_\varphi} \tag{2}$$

where τ is the response time, γ_φ is the intrinsic viscosity, P_s is the spontaneous polarization, E is the electric field strength, we can infer that the FLC+0.1wt% $BaTiO_3$ with low doping concentration and the largest spontaneous polarization under the same electric field, will have a shorter response time. On the other hand, while the spontaneous polarization of the FLC+1.0 wt% $BaTiO_3$ was greater than that of pure FLC, the larger molecular weight of the polymeric surfactant in the suspension resulted in an overall increase in viscosity. The interplay of the two led to an increase in the response time. Taking into consideration the rise and fall time performances of the different doping concentrations, we can conclude that the FLC+0.1 wt% $BaTiO_3$ is optimal.

Sample	Rise time (μs)	Fall time (μs)	Response time (μs)
pure FLC	75	360	435
FLC+0.1wt% $BaTiO_3$	30	280	310
FLC+1.0wt% $BaTiO_3$	100	370	470

Table 2. The response time of the SSFLC mode of FLC with different doping concentrations of $BaTiO_3$ suspensions.

The V-shaped switching of the SSFLC mode is shown in Figure 9, and we compared two scenarios: identical concentration but different frequencies as well as identical frequency but different concentrations. First of all, applying triangular waves of different frequencies at identical doping concentration, one can see that the hysteresis phenomenon became more pronounced with increasing frequency of the applied electric field (5 Hz to 10 Hz), resulting in a pseudo W-shaped switching. Therefore, when the curve passed through zero electric field, it was not possible to obtain a relatively dark state. There was also a phase shift in the relatively dark state, due to the fact that as the frequency of the applied electric field was increased; the liquid crystal molecules became unable to catch up with the switching frequency. On the other hand, for the V-shaped switching of triangular waves with identical frequency but different doping concentrations, the FLC+0.1 wt% $BaTiO_3$ exhibited the best V-shaped switching at 5 Hz, with no hysteresis phenomenon observable in the figure. The V-shaped switching properties of the FLC+0.1 wt% $BaTiO_3$ were superior to the pure FLC at different frequencies, proving that doping $BaTiO_3$ resulted in an enhancement of the V-shaped switching.

In particular, we examined in detail the case with an electric field applied at a frequency of 5 Hz and high doping concentration (FLC+1.0wt% $BaTiO_3$). We found that the gray scale performance were inferior to the pure FLC and FLC+0.1wt% $BaTiO_3$, but it was worth noting that the voltage required for switching between the two ferroelectric states (the region demarcated by the red dashed line in the figure) were smaller than those for the pure FLC and FLC+0.1wt% $BaTiO_3$. From this phenomenon, we can indirectly infer that doping $BaTiO_3$ in the liquid crystal materials enhances sensitivity to applied electric fields.

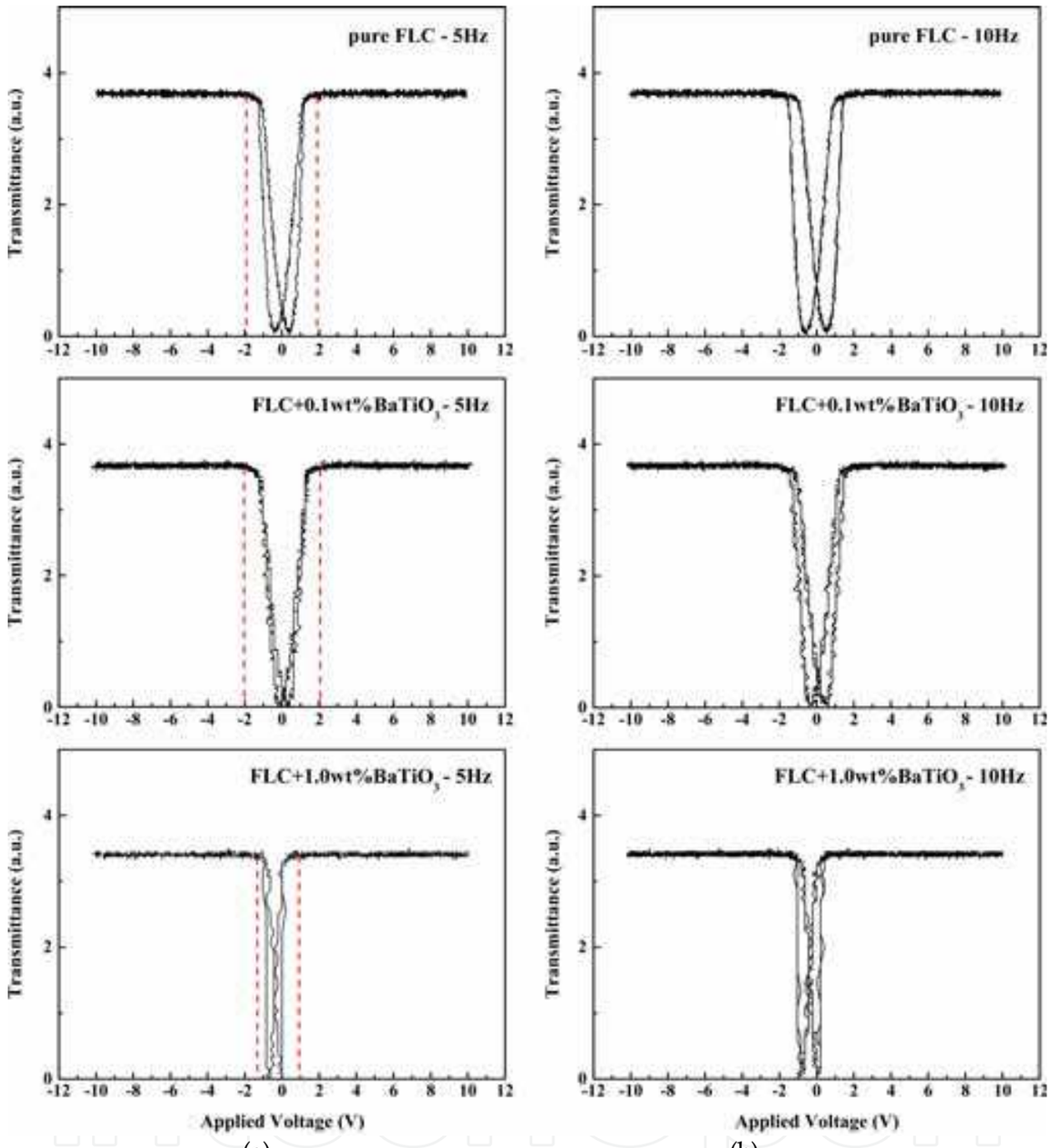

Fig. 9. The dependence of the transmittance of FLC with different doping concentrations of $BaTiO_3$ suspensions on the applied triangular waveform voltage at (a) 5 Hz and (b) 10 Hz.

(The red dashed line represents the switching between the two ferroelectric states)

3.3 Effect of doping NPs-$BaTiO_3$ on the physical and electro-optical properties of PDLC mode

The PDLC device is controlled by the micro nematic droplets, coated by the polymer matrix. To understand the effect of doping NPs-$BaTiO_3$ in the PDLC, one must first determine the changes in the physical and electro-optical properties of the NLC after doping NPs-$BaTiO_3$.

By POM and DSC measurements, we found that the nematic-isotropic transition temperatures (T_{NI}) for the samples with various concentrations were almost identical, at $T_{NI\text{-}pure}$= 83.1°C, $T_{NI\text{-}0.1wt\%}$= 81.9°C and $T_{NI\text{-}0.5wt\%}$= 79.9°C respectively. On the other hand, texture observation results revealed that a small increase in the concentration of defects occurred with increasing concentrations of NPs-$BaTiO_3$ in the NLC.

The anisotropic dielectric constants were measured using a single-cell method and were obtained from the characteristic relationship between capacitance and voltage (Wu et al., 1991). When the voltage was lower than the threshold voltage, the electric field direction was perpendicular to the liquid crystal director. The measured capacitance value is represented as $C_{\perp}$ and $\varepsilon_{\perp}$ was calculated; whereas $C_{//}$ and $\varepsilon_{//}$ were obtained by extrapolating the relationship of the capacitance and V_{th}/V, where V_{th} is the threshold voltage. From Figure 10, it can be observed that when the temperature is reduced into the range of the liquid crystal phase, $\varepsilon_{\perp}$ decreases according to the decreasing temperature, but $\varepsilon_{//}$ increases inversely. After doping NPs-$BaTiO_3$, which has a large electric dipole moment, $\varepsilon_{\perp}$ and especially $\varepsilon_{//}$ also become significantly larger. Comparing these two results, anisotropic dielectric constants increase according to the increasing concentration of the dopant, which are respectively, $\Delta\varepsilon_{\text{-}pure}$ = 13.03, $\Delta\varepsilon_{\text{-}0.1wt\%}$ = 13.88, $\Delta\varepsilon_{\text{-}0.5wt\%}$ = 14.74.

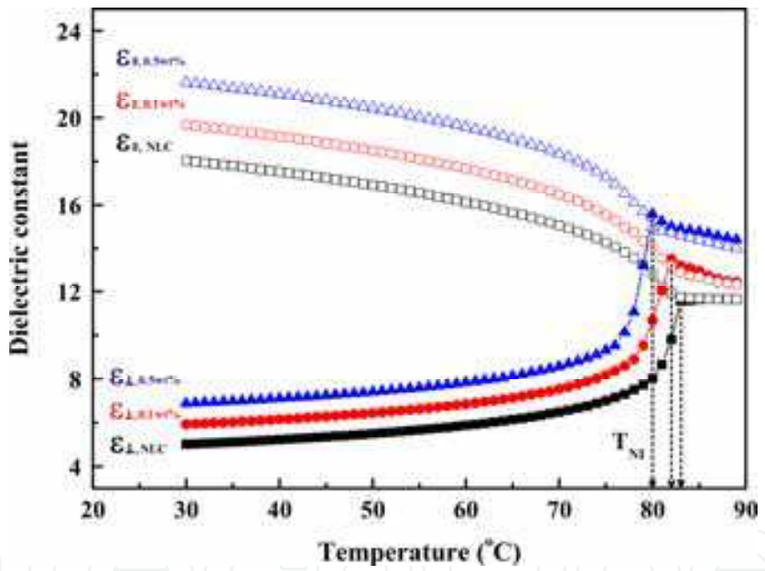

Fig. 10. The dependence of the dielectric constants ($\varepsilon_{\parallel}$ and $\varepsilon_{\perp}$) for NLC with different doping concentrations of $BaTiO_3$ suspensions on the temperature.

Next, we studied the V-T characteristics of NLC doped NPs-$BaTiO_3$. We made use of the homogeneous ECB mode to measure the threshold voltage before and after doping. The transmittance under the homogeneous ECB mode is given by the following formula (Chigrinov, 1999):

$$T = \frac{1}{2}\left[cos^2(\varphi_1 - \varphi_2) - sin2\varphi_1 sin2\varphi_2 sin^2\left(\frac{\delta}{2}\right)\right] \tag{3}$$

where φ_1 and φ_2 are the angles between the orientation direction and the two polarizers, and δ is the phase retardation. We set the polarizers such that φ_1=φ_2=45°, and in the absence of an

applied electric field, the transmittance reached its maximum and varied periodically with variations in the electric field, as shown in figure 11(a). The derived V_{th} in figure 11(b) is consistent with the V_{th} obtained from the relationship of voltage and capacitance. The results showed that, after doping, V_{th} would be 10% and 26% lower respectively compared with before doping. It was reduced from $V_{th\text{-}pure}$ = 0.95 V to $V_{th\text{-}0.1wt\%}$ = 0.85 V and finally to $V_{th\text{-}0.5wt\%}$ = 0.70 V. The threshold voltage (V_{th}) relationship for homogeneous ECB equation was used:

$$V_{th} = \pi \sqrt{\frac{K_{11}}{\varepsilon_0 |\Delta\varepsilon|}} \tag{4}$$

where K_{11} is the splay elastic constant of the NLC, ε_0 is the vacuum permittivity and $\Delta\varepsilon$ is the anisotropic dielectric constant. Using the equation to substitute for Δε and V_{th}, we calculated the splay elastic constants to be $K_{11\text{-}pure}$=10.55 pN, $K_{11\text{-}0.1wt\%}$=8.99 pN, and $K_{11\text{-}0.5wt\%}$=6.48 pN respectively. Note that the splay elastic constants changed significantly after doping.

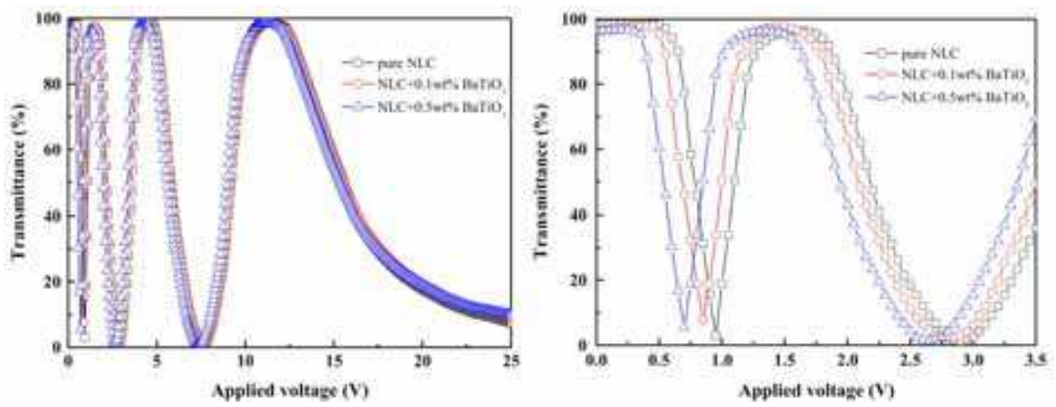

Fig. 11. Transmittance as a function of the applied voltage for NLC with different doping concentrations of $BaTiO_3$ suspensions. The demonstration range of the horizontal axis were (a) from 0 to 25 V, and (b) from 0 V to 3.5 V.

In summary, low doping concentrations of NPs-$BaTiO_3$ enhanced the physical and electro-optical properties of the NLC. The dielectric anisotropic constants, nematic-isotropic transition temperature, thershold voltage, and splay elastic constant are shown in Table 3.

Sample	Δε	V_{th} (V)	T_{NI} (°C)
pure NLC	13.03	0.95	83.2
NLC+0.1wt%$BaTiO_3$	13.88	0.85	81.9
NLC+0.5wt%$BaTiO_3$	14.74	0.70	79.9

Table 3. Comparison of dielectric anisotropy, threshold voltage, and phase transition temperatures for pure liquid crystals and liquid crystals with ferroelectric nanoparticles.

After preparation of the PDLC films, a square wave electric field (1 kHz) was applied to measure the V-T characteristics of the three PDLC films with different doping concentrations, as shown in Figure 12. All three PDLC films exhibited typical V-T

characteristics of PDLC. As the applied electric field was increased, the transmittance increased unit a saturation threshold was reached (saturated transmittance, T_s). $T_{s\text{-}pure}$ = 99.7%, $T_{s\text{-}0.1wt\%}$ = 98.9% and $T_{s\text{-}0.5wt\%}$ = 96.6%, displaying a tendency to decrease as doping concentration increases. On the other hand, the decrease in the driving voltage (V_d) was observed from the Figure 12. Although the degree of voltage decline was incomparable to the voltages during the ECB mode, doped with NPs-$BaTiO_3$, here the 0.1wt% doping and 0.5wt% doping were respectively 4% and 15% lower compared to the pure PDLC.

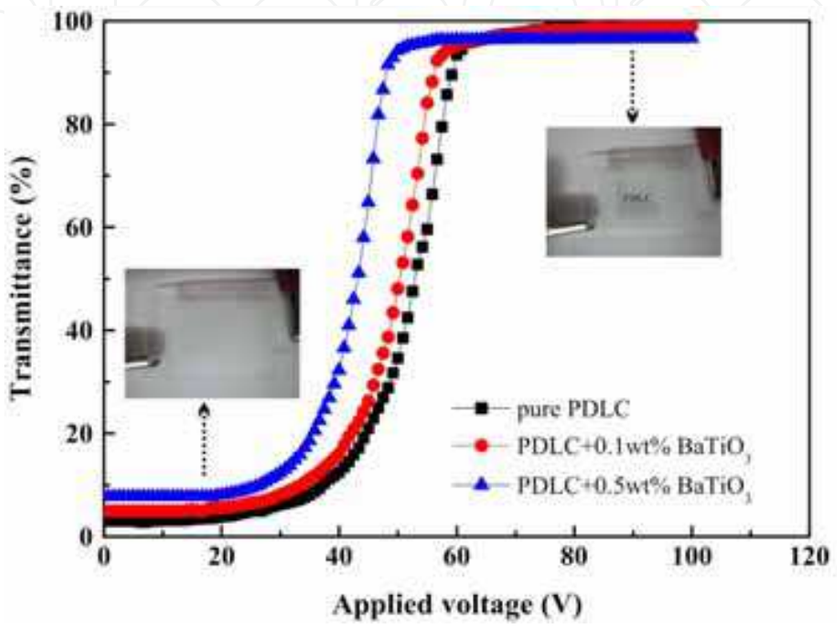

Fig. 12. The dependence of the transmittance for PDLC with different doping concentrations of $BaTiO_3$ suspensions on the applied voltage at 1 kHz. The photographs of PDLC+0.5wt% $BaTiO_3$ film are shown in the inset.

In order to understand the T_s and V_d after doping, we assessed the PIPS method. During the UV polymerization process, the increase in the polymer molecular weight led to a decrease in the immiscibility of the polymer and LC. When the immiscibility is sufficiently low, phase separation will begin. The decline in T_s with respect to increasing doping concentration indirectly confirmed that NPs-BaTiO3 was in the polymer phase during the phase separation. As the refractive index of NPs-$BaTiO_3$ (n_{NPs} = 2.42) is higher than the refractive index of the polymer (n_p = 1.52), the refractive index of the polymer would increase after doping, compared to the initial value while matching with the liquid crystal (n_p and n^o_{LC}). When the NPs-$BaTiO_3$ dopant was introduced, there was a refractive index mismatch. When the incoming light was incident in the same direction as the applied electric field (perpendicular to the cell surface), a small portion of the light was scattered, resulting in a slight decline in the value of T_s (Yaroshchuk & Dolgov, 2007). On the other hand, the driving voltage relationship for the PDLC is given as (Drzaic, 1998):

$$V_d = \frac{d}{3a}\left(\frac{\rho_p + 2}{\rho_{LC}}\right)\left[\frac{K(l^2 - 1)}{\Delta\varepsilon\varepsilon_0}\right]^{\frac{1}{2}} \tag{5}$$

where d is the layer thickness; $l=a/b$ is the ratio of a, the length of the semi-major axis, and b, the length of the semi-minor axis; K is the average elastic constant; ρ_p is the resistivity of the polymer and ρ_{LC} is the resistivity of the liquid crystal. Comparing with the results from the ECB mode, under the assumption that the NPs-$BaTiO_3$ dopant does not affect the size and shape of nematic droplet (which we will confirm in the next section), we can reasonably infer that only a portion of NPs-$BaTiO_3$ remains in the droplet after phase separation. This limits the alteration on the inversely proportional relationship of V_d to the anisotropic dielectric constant and the directly proportional relationship of V_d to the elastic constant. Summarizing the measured results of T_s and V_d, the NPs-$BaTiO_3$ dopant was in polymer phase and altered the n_p. Some part remained in the droplet and altered the physical properties of LC. The insert of Figure 12 illustrates the vertical view of the PDLC+0.5wt% $BaTiO_3$ film. When the applied voltage was below V_d, the PDLC light shutter was scattering and could block the characters behind. When the saturation voltage was applied, The shutter was transparent and the images with the characters "PDLC", which were placed at 2 cm behind the cells, were clearly visible.

The LC droplet size in PDLC is a critical factor in determining the electro-optical properties of these devices. To confirm the hypothesis of the size and shape of the droplets, the sections of the PDLC films were carried out through SEM. The SEM results indicated that the LC droplet shape was spherical and almost the same both before and after the doping. An SEM photograph of a cross section of the PDLC+0.5wt% $BaTiO_3$ film is shown in figure 13(a). The droplet sizes of different doping concentration were precisely measured and the respective number distributions N(D) are summarized in figure 13(b). The results showed that all droplet sizes have a peak distribution with average values of $D_{pure\ PDLC}$ = 2.15 ± 0.05μm, $D_{PDLC\ +0.1\ wt\%}$ = 2.15 ± 0.06μm, $D_{PDLC\ +0.5\ wt\%}$ = 2.16 ± 0.06μm. In conclusion, the effect of NPs-$BaTiO_3$ on the size and shape of droplets were not significant, which is also consistent with the inference above.

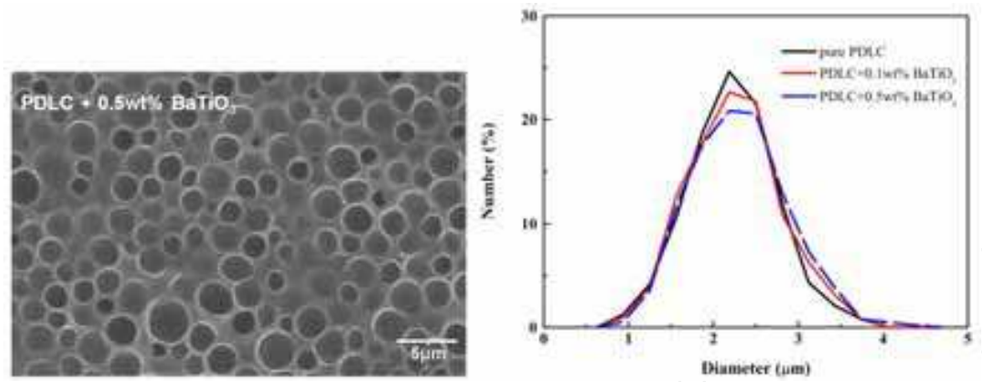

(a) (b)

Fig. 13. (a)Scanning electron microscope photograph of a cross section of the PDLC+0.5wt% BaTiO3 film. (b)The number-weighted distributions for PDLC films with different doping concentrations of $BaTiO_3$ suspensions.

Figure 14 shows the dependences of T_s on the incidence angle of the laser beam for PDLC doped with different concentrations of NPs-$BaTiO_3$. It can be clearly observed that T_s has a tendency to stay in the center of the peaks, a = 0°. As the angle between the incidence light and electric field increased, T_s decreased. When a = 90°, $T_s \approx 0\%$. For pure PDLC, as a result of material selection, the ordinary refractive index, n^o_{LC}, of the selected LC is almost identical

to the refractive index of the polymer, n_p. However, it is less than the extraordinary refractive index of LC, therefore

$$n_{LC}^{o} \approx n_p < n_{LC}^{e} \tag{6}$$

This equation creates two phenomena. The first is a high saturated transmittance that is due to the electric field effect of cell substrates in the vertical direction. Under this effect, the NLC droplets with random orientation were gradually aligned to be parallel with the electric field and n^{o}_{LC} became nearer to n_p, allowing PDLC to have high transmittance under normal light incidence. The second effect is the enhanced scattering of oblique light due to refractive index mismatches. This scattering effect becomes more obvious with increasing angles, which is recognized as an off-axis haze effect. In summary, when the equation above is met, the T_s of PDLC is more sensitive toward the changes in the angle of incident light.
As the doping concentration increased, the amount of NPs-$BaTiO_3$ in the polymer increased. Further, the refractive index of NPs-$BaTiO_3$, n_{NP}, is larger than n_p, so n_p would gradually become larger than n^{o}_{LC} after doping, giving

$$n_{LC}^{o} < n_{p-NP} < n_{LC}^{e} \tag{7}$$

Although this result gradually reduced T_s, which is similar to the V-T characteristic results in the previous section, the peak of the viewing angle becomes wider, as shown in figure. Among the experiment samples, PDLC+0.5wt% $BaTiO_3$ reduced the off-axis haze effect, and provided the best viewing performance. While PDLC+0.1wt% $BaTiO_3$ also performed better than pure PDLC, despite the lower doping concentration. Although using the modified refractive index of polymer matrix to reduce the off-axis haze effect and widen the on-state view results in a decline in T_s, it had little effect on the contrast ratio of the transparent-scattering state. The competition of these two phenomenons, introducing NPs-$BaTiO_3$ into PDLC still needs to be studied further.

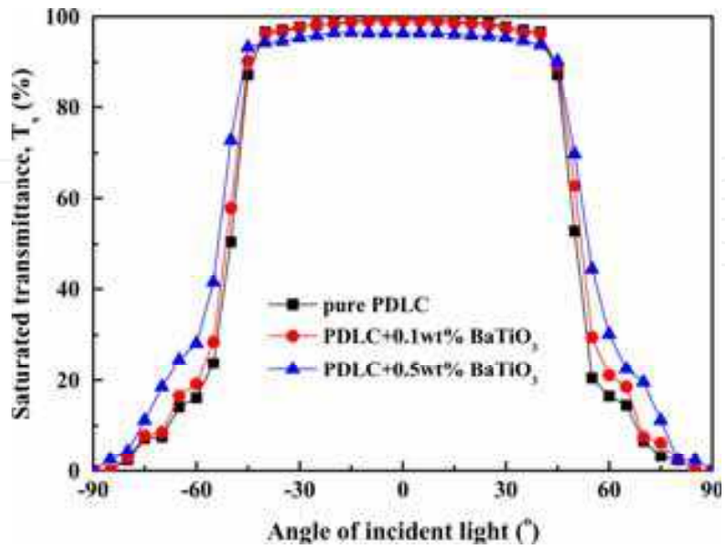

Fig. 14. The saturated transmittance T_s for PDLC films with different doping concentrations of $BaTiO_3$ suspensions as a function of the angle of incident light.

4. Conclusions

Low concentration NPs-$BaTiO_3$-doped LCD demonstrated very promising results. Without disrupting the structure and composition of the host LC, NPs-$BaTiO_3$ shares its intrinsic features with the host LC by enhancing the dielectric properties, spontaneous polarization and other vital physical properties of the host LC. This further improves the electro-optical properties of the LC device. For the case of FLC, the spontaneous polarization of FLC+ 0.1 wt% $BaTiO_3$ was about twice that of pure FLC. This also means that we can adjust the spontaneous polarization of FLC by doping with NPs-$BaTiO_3$ and eliminate the need for time-consuming molecular design and chemical synthesis. After completing the SSFLC light shutter, the V-shaped switching, response time and other electro-optical performance also have been significantly improved. Considering NLC, after doping increases in the anisotropic dielectric constants resulted in decreases in the threshold voltage in both ECB and PDLC modes. It is worth noting that part of the NPs-$BaTiO_3$ in the polymer altered the refractive index of the polymer, resulting in a wider viewing angle and improved the off-axis haze. When compared to previous methods of improve the viewing angle by placing an additional polarizer in front of the PDLC light shutter (West et al., 1992) NPs-$BaTiO_3$ doping provides better light transmittance and is more practical. In summary, using a simple doping technique to modify material properties not only provides non-chemical synthesis methods to improve the applicability of LC devices with shorter means, but also means that the drive modules for LC devices are cheaper.

5. References

Brochard, F. & de Gennes, P. G. (1970). Theory of magnetic suspensions in liquid crystals. *J. Phys. (France)*, Vol. 31, No. 7, pp. 691-708.

Chandani, A. D. L.; Hagiwara, T.; Suzuki, Y.; Ouchi, Y.; Takezoe, H. & Fukuda, A. (1988). Tristable Switching in Surface Stabilized Ferroelectric Liquid Crystals with a Large Spontaneous Polarization . *Jpn. J. Appl. Phys.*, Vol. 27, No. 5, pp. L729-L732.

Chandani, A. D. L.; Gorecka, E.; Ouchi, Y.; Takezoe, H. & Fukuda, A. (1989). Antiferroelectric Chiral Smectic Phases Responsible for the Trislable Switching in MHPOBC. *Jpn. J. Appl. Phys.*, Vol. 28, No. 7, pp. L1265-L1268.

Cheon, C. I.; Li, L.; Glushchenko, A.; West, J. L.; Reznikov, Y.; Kim, J. S. & Kim, D. H. (2005). Electro-Optics of Liquid Crystals Doped with Ferroelectric Nano-Powder, *Society for Information Display Digest of Technical Papers*, Vol. 36, pp. 1471-1473.

Chigrinov, V. G. (1999). *Liquid Crystal Devices: Physics and Applications*, Artech House Publishers, ISBN 0-89006-898-4, Boston, London.

Clark, N. A. & Lagerwall, S. T. (1980). Submicrosecond bistable electro–optic switching in liquid crystals. *Appl. Phys. Lett.*, Vol. 36, No. 11, pp. 899-891.

Crawford, G.P. & Žumer, S. (1996). *Liquid Crystals in Complex Geometries Formed by Polymer and Porous Networks*, Taylor & Francis, ISBN 0-7484-0464-3, London.

Drzaic, P. S. (1998). *Liquid Crystal Dispersions*, World Scientific, ISBN 981-02-1745-5, Singapore.

Glushchenko, A.; Cheon, C.; West, J.; Li, F.; Büyüktanir, E.; Reznikov, Y. & Buchnev, A. (2006). Ferroelectric Particles in Liquid Crystals: Recent Frontiers. *Mol. Cryst. Liq. Cryst.*, Vol. 453, pp. 227-237.

Jeng, S.-C.; Kuo, C.-W.; Wang, H.-L. & Liao, C.-C. (2007). Nanoparticles-induced vertical alignment in liquid crystal cell. *Appl. Phys. Lett.*, Vol. 91, No. 6, pp. 061112-1-3.

Kaczmarek, M.; Buchnev, O. & Nandhakumar, I. (2008). Ferroelectric nanoparticles in low refractive index liquid crystals for strong electro-optic response. *Appl. Phys. Lett.*, Vol. 92, No. 10, pp. 103307-1-3.

Kaur, S.; Singh, S. P.; Biradar, A. M.; Choudhary, A. & Sreenivas, K. (2007). Enhanced electro-optical properties in gold nanoparticles doped ferroelectric liquid crystals. *Appl. Phys. Lett.*, Vol. 91, No. 2, pp. 023120-1-3.

Kimura, S.; Kimura, S.; Nishiyama, S.; Ouchi, Y.; Takezoe, H. & Fukuda, A. (1987). Viscosity Measurement in Ferroelectric Liquid Crystals Using a Polarization Switching Current. *Jpn. J. Appl. Phys.*, Vol. 26, No. 4, pp. L255- L257.

Kobayashi, S. & Toshima, N. (2007). Nanoparticles and LCDs: It's a Surprising World. *SID.*, Vol. 9, No. 7, pp. 26-32.

Lagerwall, S. T. (1999). *Ferroelectric and Antiferroelectric Liquid Crystals*, Wiley-VCH, ISBN 3-527-29831-2, Weinheim.

Li, F.; Buchnev, O.; Cheon, C. I.; Glushchenko, A.; Reshetnyak, V.; Reznikov, Y.; Sluckin, T. J. & West, J. (2006). Orientational Coupling Amplication in Ferroelectric Nematic Colloids. *Phys. Rev. Lett.*, Vol. 97, No. 14, pp. 147801-1-4.

Li, F.; West, J.; Glushchenko, A.; Cheon, C. I. & Reznikov, Y. (2006). Ferroelectric nanoparticle/liquid-crystal colloids for display applications. *Journal of the SID.*, Vol. 14, No. 6, pp. 523-527.

Li, F.; Buchnev, O.; Cheon, C. I.; Glushchenko, A.; Reshetnyak, V.; Reznikov, Y.; Sluckin, T. J. & West, J. (2007). Erratum: Orientational Coupling Amplication in Ferroelectric Nematic Colloids. *Phys. Rev. Lett.*, Vol. 99, No. 21, pp. 219901.

Meyer, R. B.; Lievert, L.; Strzelecki, L. & Keller, P. (1975). Ferroelectric liquid crystals. *J. Physique Lett.*, Vol. 36, No. 3, pp. 69-71.

Miyama, T.; Thisayukta, J.; Shiraki, H.; Sakai, Y.; Shiraishi, Y.; Toshima, N. & Kobayashi, S. (2004). Fast Switching of Frequency Modulation Twisted Nematic Liquid Crystal Display Fabricated by Doping Nanoparticles and Its Mechanism. *Jpn. J. Appl. Phys.*, Vol. 43, No. 5A, pp. 2580-2584.

Oh-e, M. & Kondo, K. (1995). Electro–optical characteristics and switching behavior of the in–plane switching mode. *Appl. Phys. Lett.*, Vol. 67, No. 26, pp. 3895-3897.

Reznikov, Yu.; Buchnev, O.; Tereshchenko, O.; Reshetnyak, V. & Glushchenko, A. (2003). Ferroelectric nematic suspension. *Appl. Phys. Lett.*, Vol. 82, No. 12, pp. 1917-1919.

Schurian, A. & Bärner, K. (1996). Stable suspensions of ferroelectric nm-$LiNbO_3$—and nm-$PbTiO_3$—particles in hydrocarbon carrier liquids. *Ferroelectrics*, Vol. 20, No. 5. pp. 169-176.

Shiraki, H.; Kundu, S.; Sakai, Y.; Masumi, T.; Shiraishi, Y.; Toshima, N. & Kobayashi. (2004). Dielectric Properties of Frequency Modulation Twisted Nematic LCDs Doped with Palladium (Pd) Nanoparticles. *Jpn. J. Appl. Phys.*, Vol. 43, No. 8A, pp. 5425-5429.

West, J.; Fredley, S. & Carrell, J. (1992). Haze–free polymer dispersed liquid crystals utilizing linear polarizers. *Appl. Phys. Lett.*, Vol. 61, No. 17, pp. 2004-2005.

Wu, S.-T.; Coates, D. & Bartmann, E. (1991). Physical properties of chlorinated liquid crystals. *Mol. Cryst. Liq. Cryst.*, Vol. 10, No. 5, pp. 635-646.

Yaroshchuk, O. V. & Dolgov, L. O. (2007). Electro-optics and structure of polymer dispersed liquid crystals doped with nanoparticles of inorganic materials. *Opt. Mater.*, Vol. 29, pp. 1097-1102.

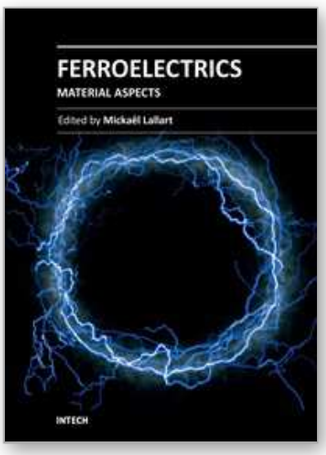

Ferroelectrics - Material Aspects

Edited by Dr. MickaÃ«l Lallart

ISBN 978-953-307-332-3
Hard cover, 518 pages
Publisher InTech
Published online 24, August, 2011
Published in print edition August, 2011

Ferroelectric materials have been and still are widely used in many applications, that have moved from sonar towards breakthrough technologies such as memories or optical devices. This book is a part of a four volume collection (covering material aspects, physical effects, characterization and modeling, and applications) and focuses on ways to obtain high-quality materials exhibiting large ferroelectric activity. The book covers the aspect of material synthesis and growth, doping and composites, lead-free devices, and thin film synthesis. The aim of this book is to provide an up-to-date review of recent scientific findings and recent advances in the field of ferroelectric materials, allowing a deep understanding of the material aspects of ferroelectricity.

InTech Europe
University Campus STeP Ri
Slavka Krautzeka 83/A
51000 Rijeka, Croatia
Phone: +385 (51) 770 447
Fax: +385 (51) 686 166
www.intechopen.com

InTech China
Unit 405, Office Block, Hotel Equatorial Shanghai
No.65, Yan An Road (West), Shanghai, 200040, China
中国上海市延安西路65号上海国际贵都大饭店办公楼405单元
Phone: +86-21-62489820
Fax: +86-21-62489821

IntechOpen